Supporting Information

Breaking the Efficiency Bottleneck of Inverted Solar Cells by Reversed Sequential Deposition

Zhipeng Yin, [‡, a, b] Beining Wang, [‡, a] Tianyu Huang, [a] Zhisheng Zhou, [b] Kang An, [b] Zsuzsanna László, [c] István Bíró, [c] Ning Li,[b,*] Hai-Qiao Wang [a, *] and Christoph J. Brabec [d, *]

[a] *Zhejiang Engineering Research Center for Fabrication and Application of Advanced Photovoltaic Materials, School of Materials Science and Engineering, NingboTech University, 315100 Ningbo, China. Email: hqwang@nbt.edu.cn*

[b] *Institute of Polymer Optoelectronic Materials & Devices, Guangdong Basic Research Center of Excellence for Energy and Information Polymer Materials, State Key Laboratory of Luminescent Materials & Devices, South China University of Technology, 510640 Guangzhou, China. Email: ningli2022@scut.edu.cn*

[c] *Institute of Technology, Institute of Biosystems Engineering, Faculty of Engineering, University of Szeged, H-6725 Szeged, Hungary*

[d] *Institute of Materials for Electronics and Energy Technology (i-MEET), Friedrich-Alexander University Erlangen-Nürnberg, 91058 Erlangen, Germany. Email: christoph.brabec@fau.de*

[‡] *These authors contributed equally to this work*

[*] Corresponding authors

Experimental section

Materials

Polymer donor PM6 and D18-Cl were purchased from Volt-Amp Optoelectronics Tech Co., Ltd and EFlexPV Limited, respectively. The acceptor L8-BO and BTP-eC9 were

purchased from Solarmer Materials Inc. Zinc acetate dihydrate ($Zn(Ac)_2 \cdot 2H_2O$) was purchased from Sigma-Aldrich. The other solvents and chemical were purchased from Energy-Chemical. All the available chemical reagents were used as received without any further purification. ZnO precursor solution was fabricated by zinc acetate dihydrate solution (50 mg/mL) in methanol.

Device fabrication

The organic solar cells (OSCs) were fabricated with an inverted structure of ITO/ZnO/Active layer/MoO_3/Ag, or normal structure of ITO/PEDOT:PSS/Active layer/PDINN/Ag. Patterned ITO glass substrates (purchased from Advanced Election Technology Co., Ltd) were ultrasonically cleaned with detergent, deionized water, and isopropanol for 30 min, respectively. Subsequently, cleaned ITO substrates were kept in an electric thermostatic drying oven at 65 °C overnight. After being treated with vacuum plasma cleaning for 120 s, a solution of ZnO was spin-coated onto the ITO substrates and annealed at 140 ºC for 20 min in air for inverted devices. For normal structure devices, a solution of PEDOT:PSS (diluted with deionized water in a vol ratio of 1:1) was spin-coated onto the ITO substrates and then annealed at 150 °C for 15 min in the air atmosphere. Then the substrates were transferred into N_2-filled glove box for deposition of active layers. The active layers of different devices were prepared according to the following processes, respectively.

For BHJ PM6:L8-BO devices, the additive TCB (10 mg/mL) was introduced into the pristine PM6:L8-BO (1:1.2 wt%, 16 mg/mL) solution. Then, the BHJ active layers were deposited by spin-coating processing under 3000 rpm for 40 s on the ITO/ZnO layers.

For LBL PM6/L8-BO devices, the PM6 solution (8 mg/mL, CF) was deposited on ITO/ZnO layers, and then the L8-BO solution (8 mg/mL, CF), with the additive of TCB (10 mg/mL), was spin-coated on the PM6 layer to form the PM6/L8-BO film.

For LBL L8-BO/PM6 devices, the L8-BO/PM6 film was formed by depositing the L8-BO first and then the PM6 layer, with identical parameters used for the PM6/L8-BO

film deposition.

For LBL D18-Cl/L8-BO devices, the D18-Cl solution (4 mg/mL, CF) was deposited on ITO/ZnO layers, and then the L8-BO solution (8 mg/mL, CF) with the additive of TCB (10 mg/mL) was spin-coated on the D18-Cl layer to form the D18-Cl/L8-BO film.

For LBL PM6/L8-BO:BTP-eC9 devices, the PM6 solution (8 mg/mL, CF) was deposited on ITO/ZnO layers and then the L8-BO:BTP-eC9 solution (0.8:0.2 wt%, 8 mg/mL, CF) with additive of TCB (10 mg/mL) was spin-coated on the PM6 layer to form the PM6/L8-BO:BTP-eC9 film.

Inverted LBL PY-IT/B1 and B1/PY-IT devices: For the LBL PY-IT/ B1 active layer, the PY-IT solution (10 mg/ml in CF) and B1 solution (10 mg/ml in CF) were spin-coated onto the ITO/ZnO substrate in sequence, under the same speed of 1750 rpm for 60 s. **For the B1/PY-IT active layer**, identical deposition conditions were applied as for the PY-IT/B1 film, but in a reversed sequence. Then the active layers were annealed at 100 °C for 10 min in a nitrogen atmosphere.

Normal LBL PY-IT/B1 and B1/PY-IT devices: the PY-IT/B1 and B1/PY-IT active layers were prepared using the same parameters as used for the inverted devices. Then the active layers were annealed at 100 °C for 10 min in nitrogen atmosphere.

BHJ PY-IT:B1 devices: A blend solution of PY-IT:B1 (1.2:1 wt%, 12 mg/ml in total in CF) was spin-coated onto the ITO/ZnO (for inverted) or ITO/PEDOT:PSS (for normal) substrates, at a speed of 2500 rpm for 30 s. Then the active layers were annealed at 100 °C for 10 min.

Top electrode and interlayer: For inverted devices, the HTL (10 nm of MoO) was deposited onto the active layer by thermal evaporation. For normal devices, the ETL was deposited from a PDINN solution (1 mg/ml in methanol) by spin-coating at a speed of 3000 rpm for 30 s. Finally, the fabrication was finished by deposition of an Ag (100

nm) electrode by thermal evaporation, with a vacuum degree of 2×10^{-7} mbar. The effective area was 0.0516 cm^2 and further defined as 0.04 cm^2 with a non-refractive mask.

Instruments and characterizations

The **UV-vis absorption spectra** were measured on a Lambda 1050+ spectrophotometer. **AFM** images were performed on an atomic force microscopy (Cypher ES) in a tapping mode. **Femtosecond transient spectroscopy (fs-TA)** spectra were measured on on a Time-Tech Spectra TA100 system, equipped with a 800 nm Femtosecond laser as light source. Lateral and vertical molecular stacking of the active layer films was analyzed using a **GIWAXS** small-angle diffractometer (Xeuss 2.0) with detector Pilatus 3R 300K. The **TEM** images were obtained on JEM-F200, equipped with EDS (Ultim Max 80). The **SEM** tests were conducted with an equipment of Sigma300, equipped with EDS Xplore30.

The **in-situ UV-vis absorption spectra** were collected by Ocean Optics QE65 Pro scientific grade spectrometer, and the light source was a combination of deuterium-tungsten halogen lamp DT-MINI-2-GS, and the analysis software was BiaoQi Spectrum Analysis Software.

The **J–V curves** were measured under a computer-controlled Keithley 2400 source meter under 100 mW cm^{-2}, AM 1.5 G solar simulator (Enlitech SS-F5). The light intensity was calibrated by a standard silicon solar cell (certified by NREL) to give a range from 0.99 to 1.01 sun. The EQE spectra were received from a commercial QE measurement system (Taiwan, Enlitech, QE-R3011).

Photostability measurement: Unencapsulated devices processed by different methods were placed in a N_2-filled chamber. For photon illumination aging, an array of white LED (spectra region: 400-800 nm, Wuhan 91PVKSolar) was used as a light source with intensity equivalent to 1 sun, which was calibrated in a way that the generated photocurrent matched the one under a solar simulator. The tested device is

continuously aged with connected in series with a fixed 500-ohm resistor.

Figures and Tables

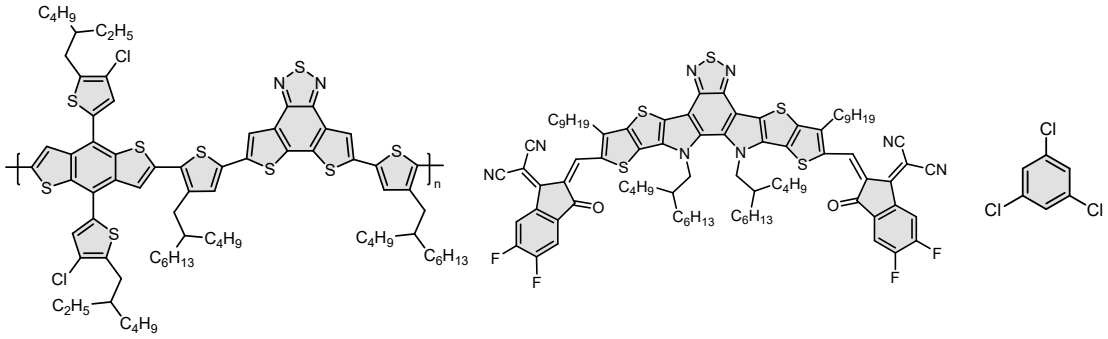

Figure S1. The chemical structure of donor D18-Cl, acceptor BTP-Ec9, and solid additive 1,3,5-Trichlorobenzene (TCB).

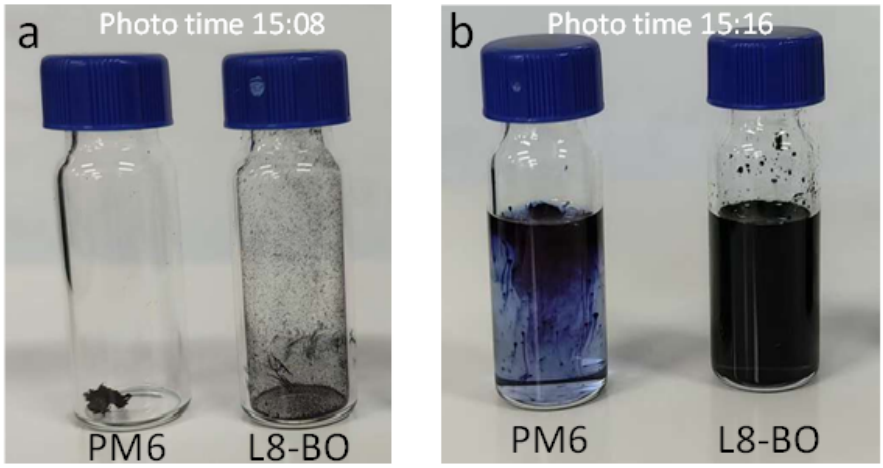

Figure S2. Dissolution-photos of the polymer PM6 and small molecule L8-BO in chloroform, before (a) and 8 minutes after (b) the addition of chloroform, demonstrating relatively low and high solubility for PM6 and L8-BO in chloroform solvent.

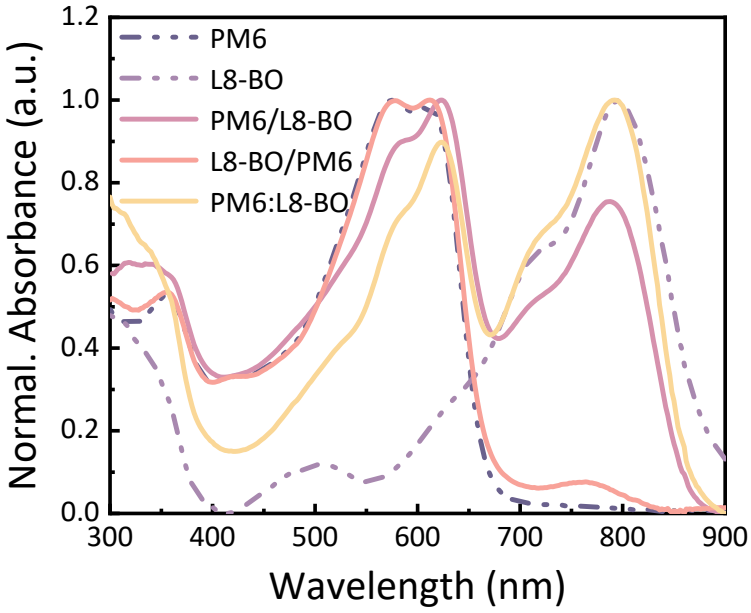

Figure S3. Normalized absorption spectra of the pure PM6, pure L8-BO, LBL PM6/L8-BO, LBL L8-BO/PM6, and BHJ PM6:L8-BO films.

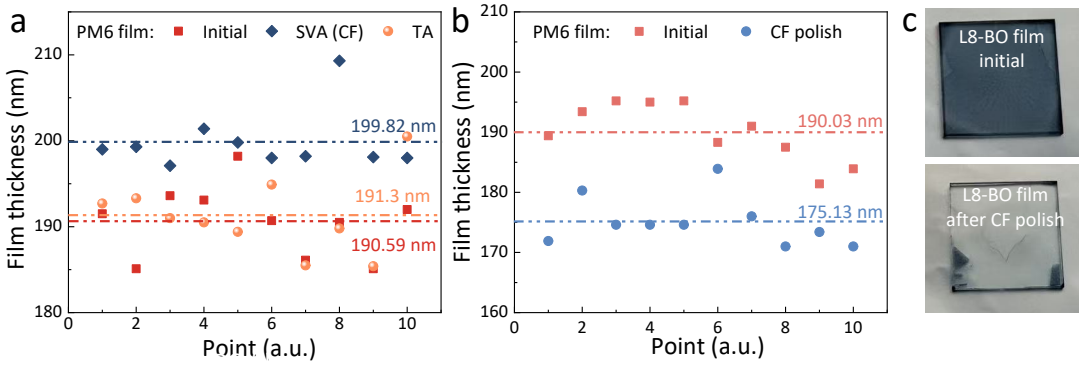

Figure S4. (a) Thickness change of PM6 film due to swelling effect by the solvent vapor annealing (SVA) of chloroform. (b) Thickness change of PM6 film due to solvent polishing by spin-coating chloroform. (c) Photos of the L8-BO film before and after chloroform polishing.

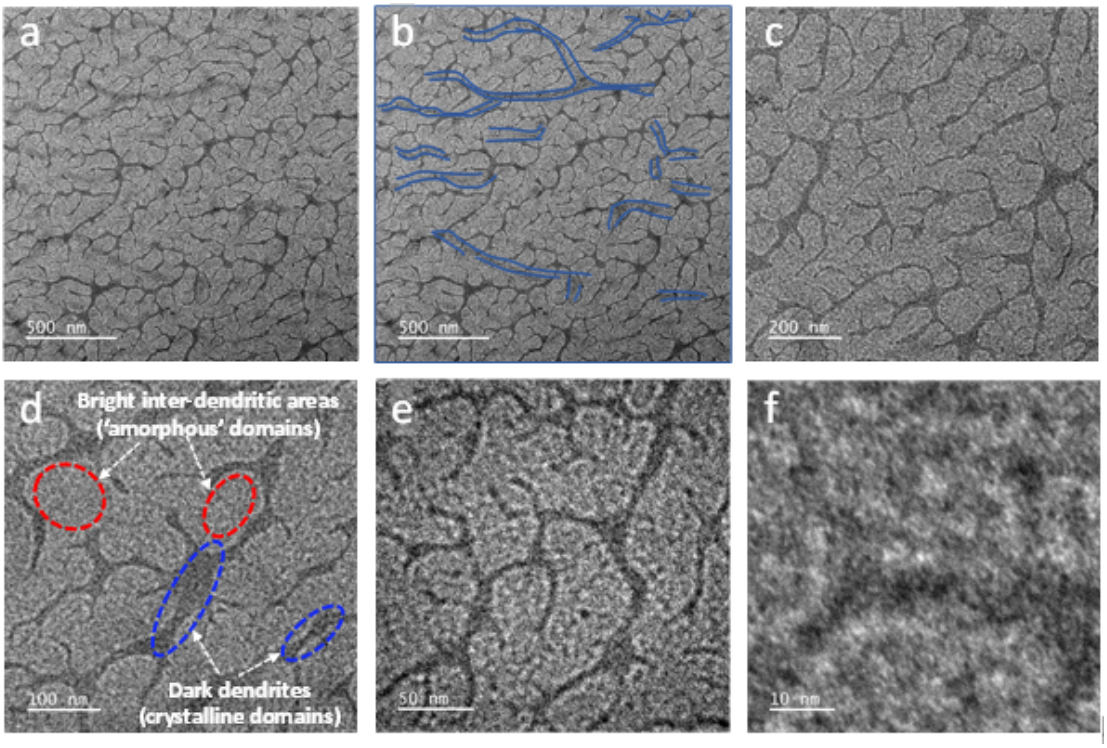

Figure S5. TEM images of the pure PM6 film obtained at different magnifications/ with different scale bars (a-f).

Bright-field TEM images of pristine PM6 film at different magnifications are presented in Figure S4. These results reveal that PM6 forms a dendritic continuous network structure upon chloroform evaporation from its solution. The darker dendritic regions (**Figure S5d**, blue circle) correspond to 'crystalline' zones of PM6, exhibiting stronger electron scattering, while the brighter inter-dendritic areas (**Figure S5d**, red circle) represent 'amorphous' or weakly crystalline zones with higher electron transmittance. Furthermore, numerous subsurface dendritic contours (**Figure S5a**) with lower electron scattering contrast (outlined in blue in **Figure S5b**) suggest that the dendritic network extends three-dimensionally throughout the PM6 film.

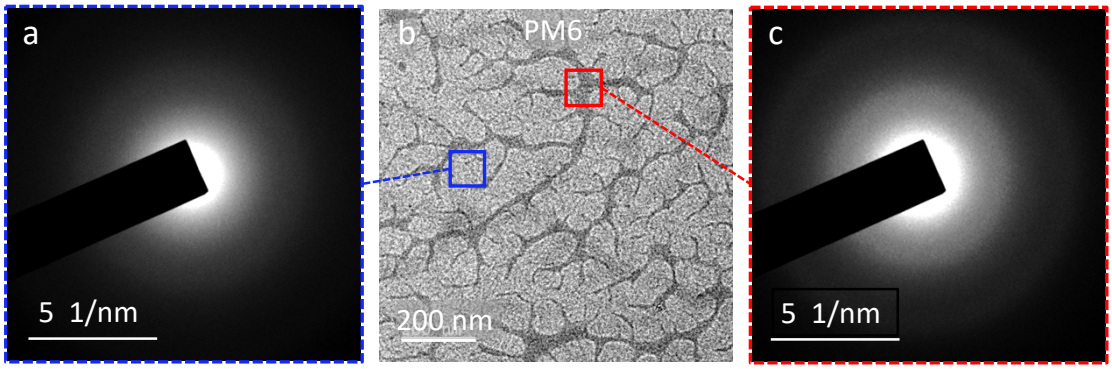

Figure S6. SAED patterns at the brighter inter-branch region (a) and dark dendritic branch (c), and TEM (b) image of the pure PM6 film.

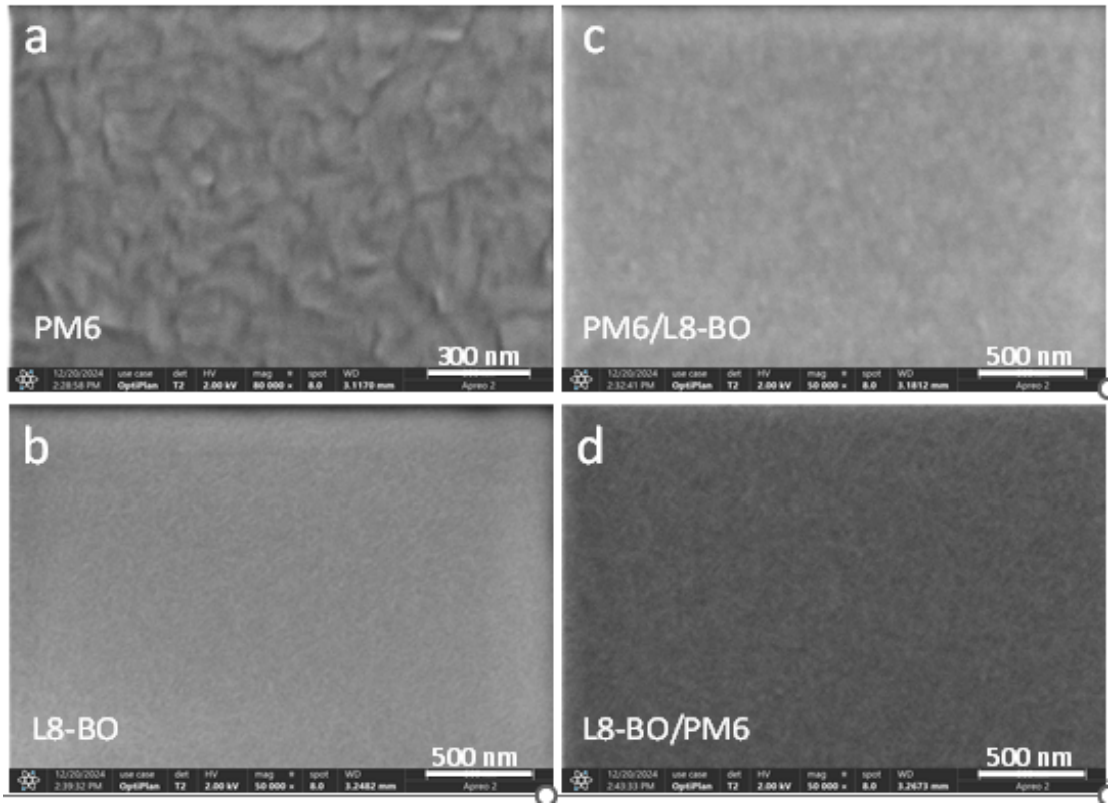

Figure S7. SEM images of the pure PM6 (a) and L8-BO (b), and LBL PM6/L8-BO (c) and L8-BO (d) films.

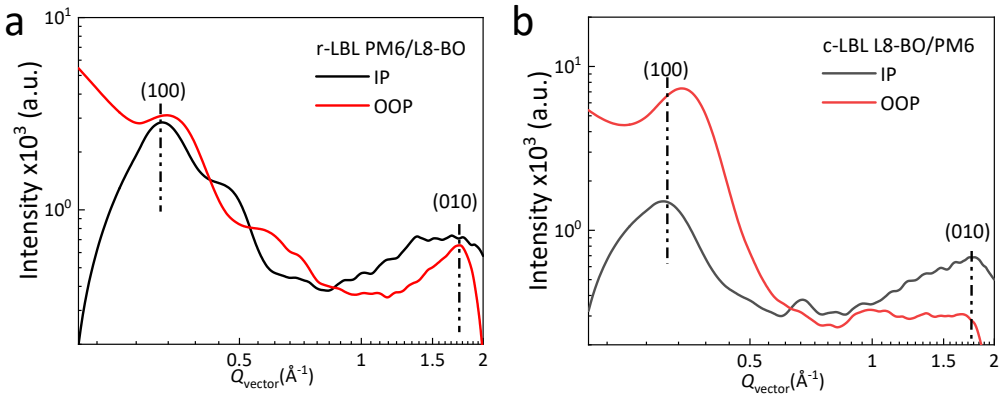

Figure S8. IP and OOP extracted line-cut profiles of the r-LBL PM6/L8-BO (a) and c-LBL L8-BO/PM6 (b) film.

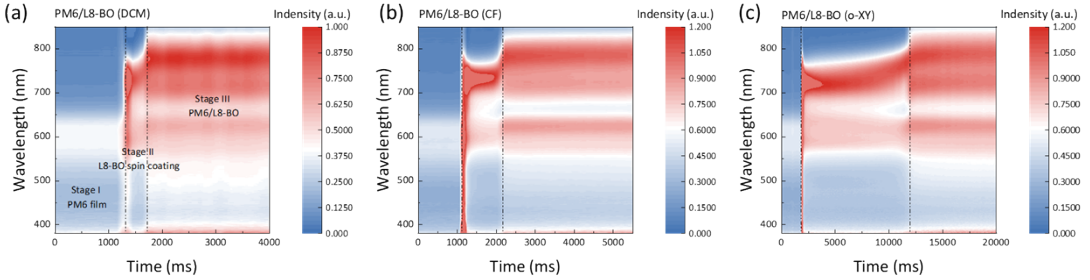

Figure S9. Time-dependent contour maps of in-situ absorption spectra of PM6/L8-BO blends, with L8-BO processed by (a) DCM, (b) CF, and (c) o-XY solution. (The PM6 was processed by CF solvent)

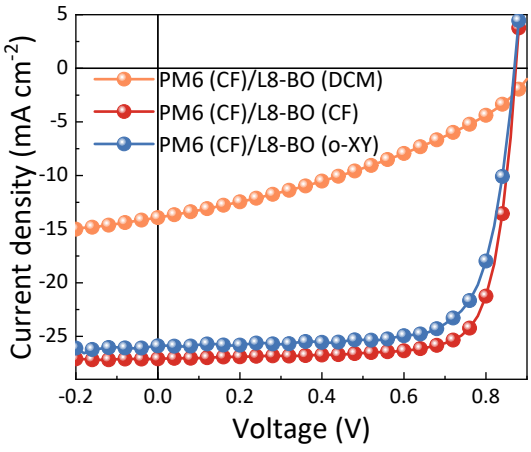

Figure S10. *J-V* curves of the inverted r-LBL PM6/L8-BO devices with L8-BO processed by different solvents.

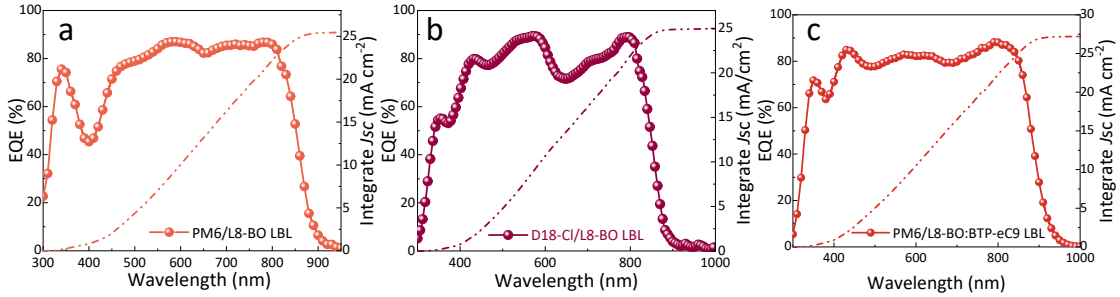

Figure S11. EQE curves of the (a) PM6/L8-BO LBL, (b) D18-Cl/L8-BO LBL, and (c) PM6/L8-BO:BTP-eC9 LBL devices.

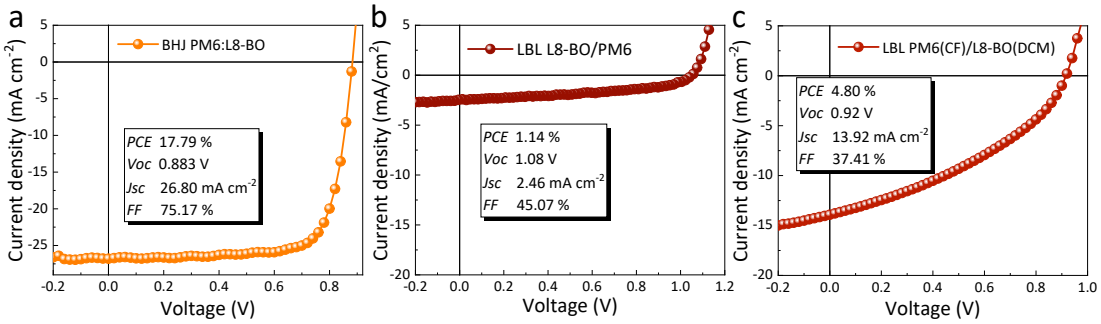

Figure S12. *J-V* curves of the control devices (with architecture of ITO/ZnO/active layer/MoO_3/Ag) based on (a) BHJ PM6:L8-BO, (b) LBL L8-BO/PM6, and (c) LBL PM6 (CF)/L8-BO (DCM) active layers, with insert of key parameters.

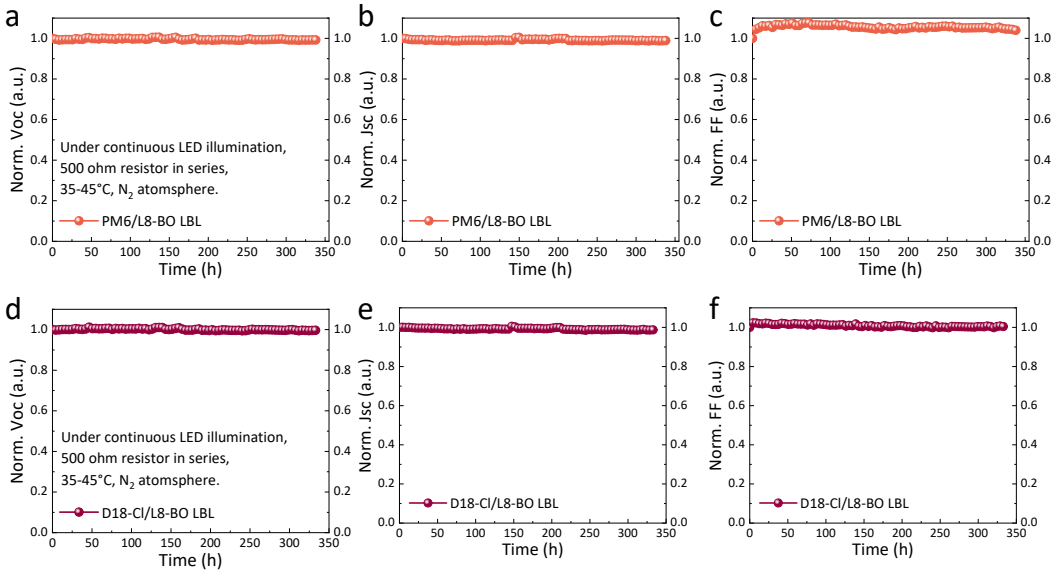

Figure S13. Operational stability of the unencapsulated LBL inverted cells under continuous LED illumination in N_2 atmosphere (temperature 35-45°C): (a, b, and c). V_{OC}, J_{SC} and FF of PM6/L8-BO cell; (d, e, and f). V_{OC}, J_{SC} and FF of D18-Cl/L8-BO cell.

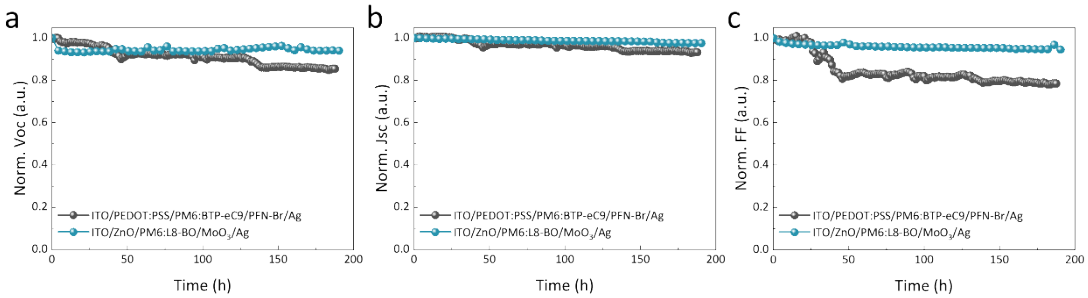

Figure S14. Operational stability of the unencapsulated BHJ cells under continuous LED illumination in N_2 atmosphere (temperature 35-45℃): (a, b, and c). V_{OC}, J_{SC} and FF of inverted PM6:L8-BO and normal PM6:BTP-eC9 BHJ cells.

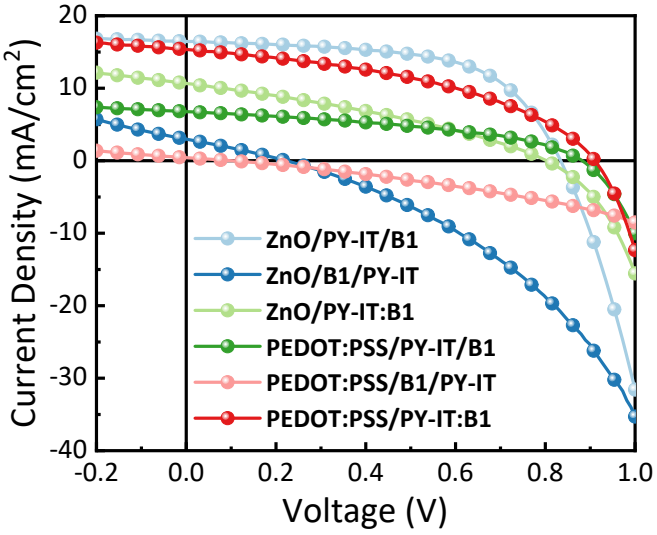

Figure S15. The *J-V* curves of different cells based on small-molecule donor and polymer acceptor systems in different device architectures, denoted as ZnO/PY-IT/B1, ZnO/B1/PY-IT, ZnO/PY-IT:B1, PEDOT:PSS/PY-IT/B1, PEDOT:PSS/B1/PY-IT, and PEDOT:PSS/PY-IT:B1, tested under illumination of AM 1.5 G 100 mW cm^{-2}.

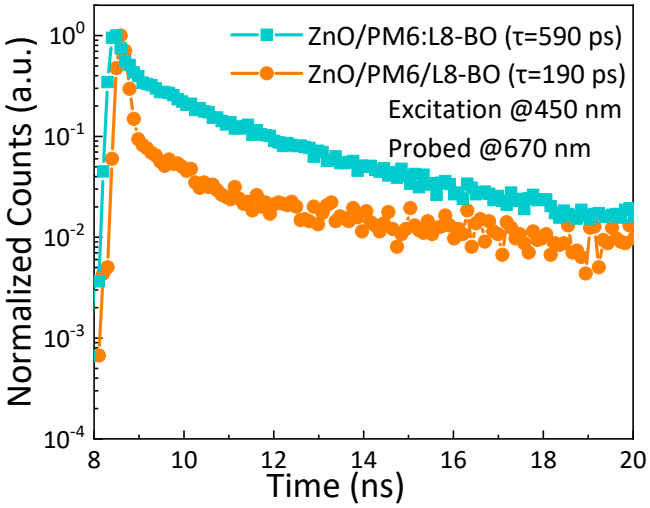

Figure S16. Time-resolved photoluminescence (TRPL) spectra of the LBL PM6/L8-BO and BHJ PM6:L8-BO films on glass/ZnO substrates. Excitation: 450 nm; probed at 670 nm.

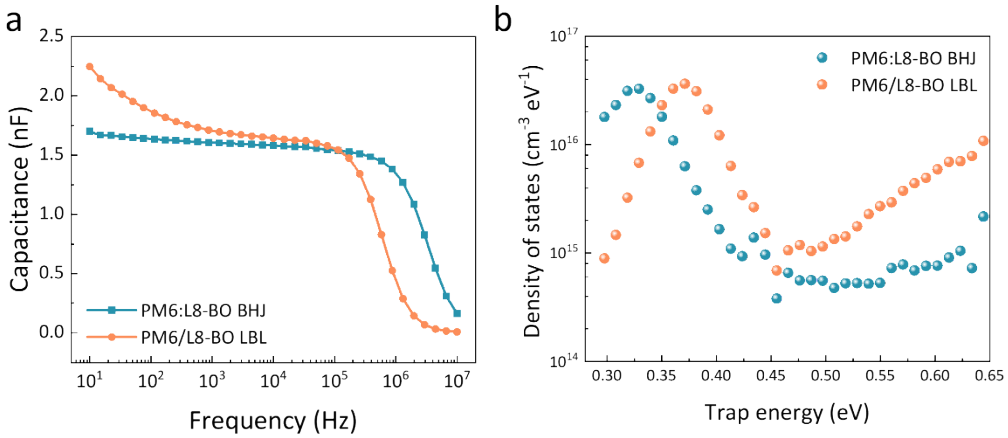

Figure S17. The capacitance versus applied voltage and trap density of state for the BHJ PM6:L8-BO and LBL PM6/L8-BO OSCs.

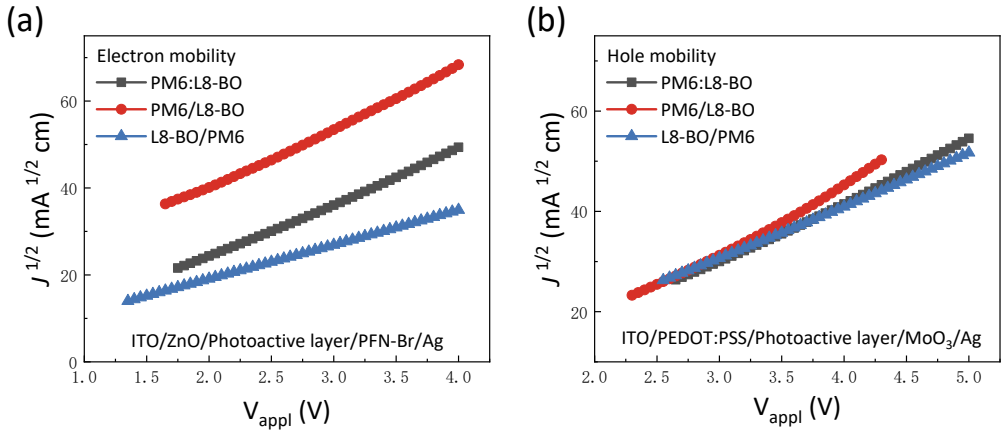

Figure S18. $J^{1/2}$-V_{appl} characteristics of electron-only (a) and hole-only (b) devices, with BHJ, r-LBL, and c-LBL blend as active layers, respectively.

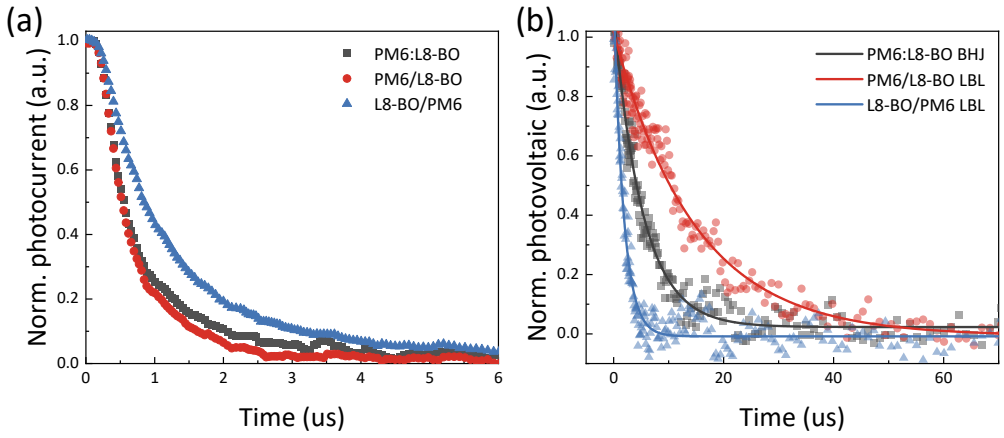

Figure S19. (a) Transient photocurrent (TPC) and transient photovoltaic (TPV) characteristics of the inverted (ITO/ZnO/photoactive layer/MoO_3/Ag) OSCs, with different photoactive layers.

Table S1. Investigations of the morphology parameters extracted from the GIWAXS measurements of PM6/L8-BO, and L8-BO/PM6 film.

Deposition	(010) in OOP				(100) in IP			
	q (Å^{-1})	d[a] (Å)	FWHM (Å^{-1})	CL[b] (Å)	q (Å^{-1})	d[a] (Å)	FWHM (Å^{-1})	CL[b] (Å)
PM6/L8-BO	1.75	3.59	0.279	20.27	0.32	19.63	0.091	61.94
L8-BO/PM6	1.67	3.76	0.883	6.40	0.31	20.40	0.085	66.37

a) Calculated from the equation: d-spacing = 2π/q.

b) Obtained from the Scherrer equation: CL = 2πK/FWHM, where FWHM is the full-width at half-maximum and K is a shape factor (K = 0.9 here).

Table S2. The Hansen solubility parameters (δ_D, δ_P, and δ_H), the relative energy difference (RED) between solvents and PM6, and boiling point of the solvents. The solutions' data are from software HSPiP. The PM6 data are from ref. [Nat. energy 2023, 8, 62].

	δ_D (MPa$^{1/2}$)	δ_P (MPa$^{1/2}$)	δ_H (MPa$^{1/2}$)	RED	b.p. (°C)
PM6	18.4	3.54	2.93	—	
DCM	17	7.3	7.1	0.78	40
CF	17.8	3.1	5.7	0.38	61

o-XY	17.8	2.5	2.9	0.20	144

Table S3. Photovoltaic parameters of the LBL PM6/L8-BO devices, with L8-BO processed by the different solvents, tested under AM1.5 G 100 mW cm^{-2} illumination.

Active layer	V_{OC} (V)	J_{SC} (mA cm^{-2})	FF (%)	PCE (average) (%)
PM6/L8-BO (DCM)	0.92	13.92	37.41	4.80 (4.04 ± 0.28)
PM6/L8-BO (CF)	0.87	27.10	77.99	18.44 (18.03 ± 0.11)
PM6/L8-BO (o-XY)	0.87	25.88	74.53	16.77 (16.23 ± 0.21)

Table S4. Reference summary of the efficient inverted BHJ and LBL OSCs.

Label	**PCE (%)**	**Inverted type**	**Ref.**
2021 PSS	14.4	LBL	Phys. Status Solidi-R **2021**, 15, 2100386
2023 AOM	15.25	LBL	Adv. Opt. Mater. **2023**, 12, 2302548
2023 AEM (blade-coated)	17.01	LBL	Adv. Energy Mater. **2023**, 13, 2203496
2025 APL Energy (slot-die coated)	13.5	LBL	APL Energy **2025**, 3, 036101
2023 Small	18.43	BHJ	Small **2024**, 20, 2311339
2024 Angewandte Chemie	18.27	BHJ	Angew. Chem. Int. Ed. **2025**, 64, e202415440
2024 AEM	18.32	BHJ	Adv. Energy Mater. **2026**, 16, 2404297
2024 AM	18.72	BHJ	Adv. Mater. **2024**, 36, 2413317
2024 JACS	18.75	BHJ	J. Am. Chem. Soc. **2024**, 146, 3363
2024 Small	18.87	BHJ	Small **2024**, 20, 2404066
2024 AFM	19.07	BHJ	Adv. Funct. Mater. **2024**, 34, 2409699
2025 Nature Photonics	18.47	BHJ	Nat. Photonics **2025**, 19, 195
2025 JACS	18.51	BHJ	J. Am. Chem. Soc. **2025**, 147, 6763
2025 AFM	19.51	BHJ	Adv. Funct. Mater. **2025**, 35, 2504623
2026 AM	19.06	BHJ	Adv. Mater. **2026**, n/a, e22299. DOI: 10.1002/adma.202522299

Table S5. Parameters of devices based on different polymer donors and small molecule acceptors. The average PCEs are obtained based on 8 individual cells.

Active layer	V_{OC} [V]	J_{SC} [mA cm^{-2}]	FF [%]	PCE (average) [%]
PM6 single layer	1.05	0.56	56.43	0.33 (0.31±0.02)
PM6:L8-BO BHJ	0.88	26.80	75.17	17.79 (17.15±0.33)
L8-BO/PM6 LBL	1.08	2.46	45.07	1.14 (0.99±0.15)
PM6/L8-BO LBL	0.87	27.10	77.99	18.44 (18.03±0.11)
D18-Cl/L8-BO LBL	0.90	26.70	78.15	18.71 (18.35±0.13)
PM6/L8-BO:BTP-eC9 LBL	0.88	28.28	77.33	19.20 (18.80±0.21)

Table S6. Parameters of devices based on small-molecule donor B1 and polymer acceptor PY-IT, in different architectures.

Devices	V_{OC} [V]	J_{SC} [mA cm^{-2}]	FF [%]	PCE [%]	R_S [Ω cm^2]	R_{Sh} [Ω cm^2]
ZnO/PY-IT/B1	0.83	16.45	59.83	8.20	123.46	8569.39
ZnO/B1/PY-IT	0.22	2.97	27.34	0.18	1675.35	2883.93
ZnO/PY-IT:B1	0.80	10.65	32.94	2.82	504.98	2084.205
PEDOT:PSS/PY-IT/B1	0.88	6.76	42.07	2.51	340.87	5419.66
PEDOT:PSS/B1/PY-IT	0.09	0.42	25.64	0.01	3672.74	3930.86
PEDOT:PSS/PY-IT:B1	0.91	15.35	42.98	6.00	179.37	3183.23

Table S7. Summary of electron and hole mobility values obtained from the electron-only (ITO/ZnO/blend/PFN-Br/Ag) and hole-only (ITO/PEDOT:PSS/blend/MoO_3/Ag) devices, with different photoactive blends. (The μ_e and μ_h were evaluated by the SCLC method according to Ref. Adv. Mater. 2016, 28, 7405)

Active layer	μ_e ($\cdot 10^{-4}$ cm^2 V^{-1} s^{-1})	μ_h ($\cdot 10^{-4}$ cm^2 V^{-1} s^{-1})	μ_e/μ_h
PM6:L8-BO	5.06	4.84	1.05
PM6/L8-BO	6.28	6.01	1.04
L8-BO/PM6	2.07	3.62	0.57

Table S8. Summary of TPV and TPC lifetimes of the devices with different photoactive layers.

Photoactive layer	TPV lifetime (μs)	TPC lifetime (μs)
PM6:L8-BO	5.26	0.604
PM6/L8-BO	14.62	0.619
L8-BO/PM6	1.80	0.976